Next-to-leading-logarithmic QCD corrections to the cross section $\sigma(e^+e^- \to t\bar{t}H)$ at 500 GeV

Cailin Farrell* and André H. Hoang†

Max-Planck-Institut für Physik (Werner-Heisenberg-Institut), Föhringer Ring 6, 80805 München, Germany

We determine the next-to-leading logarithmic (NLL) QCD corrections to the cross section $\sigma(e^+e^- \to t\bar{t}H)$ for center-of-mass (c.m.) energies up to 500 GeV. The dynamics is dominated by nonrelativistic effects, and the summation of terms singular in the relative $t\bar{t}$ velocity is mandatory to all orders in the strong coupling constant α_s using an effective theory. The summations lead to an enhancement of the tree-level predictions by about a factor of 2 and are important for the determination of the top Yukawa coupling. We also study the impact of polarization of the electron-positron beams and provide a fast approximation formula for the known $\mathcal{O}(\alpha_s)$ QCD fixed-order prediction.

I. INTRODUCTION

The discovery and exploration of the mechanism of mass generation and electroweak symmetry breaking is one of the most important tasks of future collider experiments. Within the standard model of elementary particle physics (SM) electroweak symmetry breaking is realized by the Higgs mechanism which postulates the existence of an electric neutral elementary scalar field that interacts with all SM particles carrying nonzero hypercharge and weak isospin. Through self-interactions this Higgs field acquires a vacuum expectation value $V = (\sqrt{2}G_F)^{1/2} \approx$ 246 GeV, G_F being the Fermi constant, which breaks the $SU(2)_L \times U(1)_Y$ symmetry at high energies down to the electric $U(1)_{\text{em}}$ below the symmetry breaking scale and leads to nonzero masses of the elementary particles. The Higgs mechanism also predicts that the Higgs fields can be produced as a massive Bose particle in collider experiments if sufficient energy is provided in the process. The mass of the Higgs boson is expected to lie between the current experimental lower limit of 114.4 GeV [1] and about 1 TeV. Current analyses of electroweak precision observables yield a 95% CL upper indirect bound of 186 GeV for the Higgs boson mass [2]. While a Higgs boson with a mass up to 1 TeV can be found at the LHC, precise and model-independent measurements of quantum numbers and couplings are likely to be restricted to a future e^+e^- linear collider [3–5] such as the International Linear Collider (ILC) project.

The Higgs mechanism predicts that the quark masses m_q are related to the quark-Higgs Yukawa coupling λ_q through the relation $m_q = \lambda_q V$. This makes the measurement of the Yukawa coupling to the top quark ($m_t = 172.5 \pm 2.3$ GeV [6]) particularly important since it is expected to have a high precision. At a future e^+e^- linear collider the top Yukawa coupling can be measured from the process

$e^+e^- \to t\bar{t}H$ since the amplitudes describing Higgs radiation off the $t\bar{t}$ pair dominate the cross section.[1]

For the second phase of the ILC project with c.m. energies between 500 GeV and 1 TeV and assuming a Higgs mass of around 120 GeV the total cross section $\sigma(e^+e^- \to t\bar{t}H)$ is at the level of 1–2 fb and measurements of λ_t with experimental errors of around 5% are expected [7,8]. The precision motivates the computation of radiative corrections. In the approximation that the top quark and the Higgs boson are stable particles[2] the tree-level cross section was determined already some time ago in Refs. [10]. The full set of one-loop QCD corrections were obtained in Ref. [11]. Earlier studies using approximations were given in Refs. [12,13]. One-loop electroweak corrections were studied in Refs. [14,15] and also in Ref. [16].

The phase space region where the Higgs energy is close to its upper endpoint,

$$E_H \approx E_H^0 \equiv (s + m_H^2 - 4m_t^2)/(2\sqrt{s}), \tag{1}$$

$\sqrt{s}$ being the center-of-mass energy, was studied in detail in Ref. [17]. In the large Higgs energy endpoint region the $t\bar{t}$ pair is forced to become collinear and to move opposite to the Higgs direction in order to maximize the momentum necessary to balance the large Higgs momentum, see Fig. 1. Thus the $t\bar{t}$ invariant mass is close to $2m_t$. In this kinematic regime the $t\bar{t}$ pair is nonrelativistic in its c.m. frame and fixed-order QCD perturbation theory in powers of α_s leads to singular terms proportional to $(\alpha_s/v)^n$ and $(\alpha_s \ln v)^n$ which have to be summed to all order. Here, $v = (1 - 4m_t^2/Q^2)^{1/2}$ is the top quark relative velocity in the $t\bar{t}$ c.m. frame and Q is the $t\bar{t}$ invariant mass. In Ref. [17] these singularities were summed at NLL order in a simultaneous expansion in α_s and v and also accounting for the finite top quark width. The computations were carried out using a

---

*Electronic address: farrell@mppmu.mpg.de
†Electronic address: ahoang@mppmu.mpg.de

---

[1]An indirect measurement through virtual Higgs effects might be also possible at the $t\bar{t}$ threshold if the Higgs mass is close to the present lower experimental limit [3].

[2]For a light Higgs boson this is an excellent approximation. For $m_H = 115(150)$ GeV one finds $\Gamma_H = 0.003(0.017)$ GeV [9]
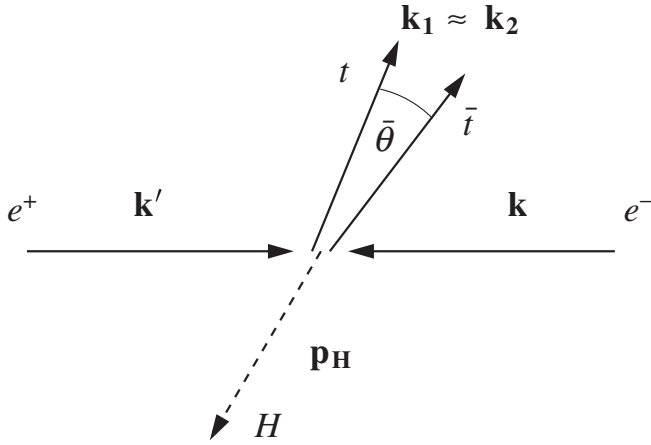
FIG. 1. Typical constellation of momenta for the process $e^+e^- \to t\bar{t}H$ in the large Higgs energy endpoint region.

nonrelativistic effective theory [18–20] originally developed for the threshold region in the process $e^+e^- \to t\bar{t}$. Because of the large top quark width, $\Gamma_t \approx 1.5$ GeV, the nonrelativistic $t\bar{t}$ dynamics is protected from nonperturbative effects and the summations can be carried out with perturbative methods. It was shown in Ref. [17] that the summation of the singular terms leads to an enhancement of the total cross section that needs to be accounted for up to c.m. energies of about 700 GeV. The impact of the summations increases with the fraction of the phase space where the c.m. top velocity v is nonrelativistic, i.e. it increases with the Higgs and top quark masses and decreases with the c.m. energy. A convenient measure for the impact of the nonrelativistic summations on the total cross section is the maximal relative velocity of the $t\bar{t}$ pair which is achieved at the *low* Higgs energy endpoint $E_H = m_H$,

$$v^{\mathrm{max}} = \left(1 - \frac{4m_t^2}{Q_{\mathrm{max}}^2}\right)^{1/2} = \left(1 - \frac{4m_t^2}{(\sqrt{s} - m_H)^2}\right)^{1/2}. \quad (2)$$

For small v^{max} the summations have a large effect since the available phase space is predominantly nonrelativistic.

As was already demonstrated in Ref. [17], the fixed-order QCD predictions [11–13] become unreliable for c.m. energies up to 500 GeV, which corresponds to the energy available during the first phase of the ILC project. For $m_H = (120, 130, 140)$ GeV, $m_t = 175$ GeV, and $\sqrt{s} = 500$ GeV one has $v^{\mathrm{max}} = (0.39, 0.32, 0.23)$ and consequently the entire phase space is governed by the nonrelativistic QCD dynamics. The nonrelativistic expansion based on the parametric counting $\alpha_s \sim v \ll 1$ has to be employed rather then the α_s expansion to make reliable theoretical predictions for the cross section. Another consequence of small v^{max} is that the cross section for c.m. energies up to 500 GeV can be substantially smaller than 1 fb due to phase space suppression, which severely restricts statistics. Since the singularities proportional to $(\alpha_s/v)^n$ and $\alpha_s \ln v$ are large in this case only predictions

where the nonrelativistic summations are accounted for allow for a realistic assessment of Yukawa coupling measurements during the first phase of the ILC project [21,22].

In this work we give a detailed analysis of the total cross section and the Higgs energy distribution for the process $e^+e^- \to t\bar{t}H$ for c.m. energies up to 500 GeV accounting for QCD effects at NLL order in the nonrelativistic expansion. The approach of Ref. [17] developed for descriptions of the large Higgs energy endpoint region is extended to the case where the entire phase space is nonrelativistic. We show that our NLL order predictions are substantially larger than the known tree-level predictions, which have in fact been used for experimental simulations studies at 500 GeV in the past [21]. We also account for the possibility of electron-positron beam polarization which can further enhance the cross section. Our results significantly affect the prospects for top Yukawa coupling measurements during the first phase of the ILC project.

The content of this paper is organized as follows: In Sec. II we review the ingredients of the factorization formula derived in Ref. [17] in the large Higgs energy endpoint region valid for large c.m. energies. We extend the presentation by also accounting for electron-positron beam polarization and by giving a more detailed discussion of the $t\bar{t}$ final state in the helicity basis. In Sec. III we discuss the modifications that need to be applied to the factorization formula for the case where the full phase space is nonrelativistic. In Sec. IV we analyze our results numerically and Sec. V contains the conclusion.

II. THE LARGE HIGGS ENERGY ENDPOINT REGION

In the large Higgs energy region $E_H \approx E_H^0$ the Higgs energy distribution can be factorized into a hard part describing the production of the $t\bar{t}$ pair and the Higgs boson and in a low-energy part describing the nonrelativistic dynamical QCD effects of the $t\bar{t}$ subsystem. The latter are responsible for the singularities proportional to powers of α_s/v and $\alpha_s \ln v$. The factorization formula, valid at NLL order for unpolarized electron-positron beams and top quarks, was derived in Ref. [17]. Accounting for electron-positron beam polarization and polarized top quarks the factorization formula for fully polarized electrons and positrons has the form

$$\left(\frac{d\sigma}{dE_H}(E_H \approx E_H^0)\right)^{\pm}$$

$$= \frac{8N_c[(1 + x_H - 4x_t)^2 - 4x_H]^{1/2}}{s^{3/2}m_t^2}$$

$$\times \left(c_0^2(v)F_{0,\pm}^Z + \sum_{i=-1,0,+1} c_{(1,i),\pm}^2(v)F_{(1,i),\pm}^{\gamma Z}\right)$$

$$\times \mathrm{Im}[G^c(C_F\alpha_s(m_t v), v, m_t, v)], \quad (3)$$

with

$$x_t \equiv \frac{m_t^2}{s}, \qquad x_H \equiv \frac{m_H^2}{s}, \qquad x_Z \equiv \frac{m_Z^2}{s}. \qquad (4)$$

Here, c_0 and $c_{(1,i)}$ are the hard singlet and triplet QCD Wilson coefficients which depend on the effective theory renormalization parameter ν, $F_{0,\pm}^Z$ and $F_{(1,i),\pm}^{\gamma Z}$ are the hard electroweak tree-level matching conditions, and G^c is the Green's function of the NLL Schrödinger equation of the effective theory for the top quarks. A detailed discussion of these quantities will follow shortly.

The index denotes the helicity of the electrons, i.e. "$-$" refers to right-handed positrons and left-handed electrons and the index "$+$" refers to left-handed positrons and right-handed electrons. Since the electron mass is neglected, the cross section vanishes if both electron and positron have the same helicity. For arbitrary polarization P_+ of the positrons and P_- of the electrons the spectrum reads

$$\left(\frac{d\sigma}{dE_H}\right) = \frac{1}{4}(1+P_-)(1-P_+)\left(\frac{d\sigma}{dE_H}\right)^+$$
$$+ \frac{1}{4}(1-P_-)(1+P_+)\left(\frac{d\sigma}{dE_H}\right)^-, \qquad (5)$$

where the polarization of a beam with N_+ right-handed particles and N_- left-handed particles is defined as

$$P = \frac{N_+ - N_-}{N_+ + N_-} \equiv \frac{N_+ - N_-}{N_{\text{tot}}} \qquad (6)$$

and can take on values between -1 and 1.

The first two terms is Eq. (3) are the hard factors and the third term is the imaginary part of the zero-distance Green function of the NLL Schrödinger equation that can be derived from the effective theory Lagrangian. The Green function describes the effects of the low-energy nonrelativistic dynamics on the $t\bar{t}$ production rate for the top pair being in an S-wave state and does not depend on the polarization of the electron-positron beams. It depends on the effective theory renormalization scaling parameter ν and is proportional to the time-ordered product of the effective theory operators describing the nonrelativistic QCD dynamics for the production and annihilation of the $t\bar{t}$ pair at leading logarithmic (LL) and NLL order.[3] At LL order (in dimensional regularization) the Green function has the simple analytic form

---

[3]The renormalization scaling parameter ν has mass dimension zero and is used in the effective theory to describe the correlated running of soft and ultrasoft fluctuations [18]. The hard effective theory matching scale (at the top quark mass) is at $\nu = 1$ and low-energy matrix elements are evaluated for $\nu \sim v \sim \alpha_s$ to avoid the appearance of large logarithmic terms.

$$G_{\text{LL}}^c(a, v, m_t, \nu) = \frac{m_t^2}{4\pi}\left\{iv - a\left[\ln\left(\frac{-iv}{\nu}\right) - \frac{1}{2} + \ln 2 + \gamma_E\right.\right.$$
$$\left.\left. + \psi\left(1 - \frac{ia}{2v}\right)\right]\right\} + \frac{m_t^2 a}{4\pi}\frac{1}{4\epsilon}. \qquad (7)$$

For the NLL order Green function we use the numerical techniques and codes of the TOPPIC program developed in Ref. [23] (see also Ref. [24]) and determine an exact solution of the full NLL Schrödinger equation employing the approach of Refs. [20]. We estimate the QCD uncertainties in the normalization of the Higgs energy spectrum from the NLL order Green function as 5% [17,25]. Note that we account for the top quark finite lifetime by shifting the $t\bar{t}$ invariant mass Q used in the Green function into the complex plane such that the top quark relative velocity reads

$$v = \sqrt{\frac{Q - 2m_t - 2\delta m_t(\nu) + i\Gamma_t}{m_t}}, \qquad (8)$$

where

$$Q^2 = s + m_H^2 - 2\sqrt{s}E_H. \qquad (9)$$

This accounts for the top quark finite lifetime consistently at LL order, see for example [26]. A consistent NLL description of finite lifetime effects and electroweak corrections shall be included in a subsequent publication. The term δm_t in Eq. (8) is a residual mass term that has to be specified perturbatively at each order to fix which top quark mass definition is being employed. In the pole mass scheme the residual mass term vanishes to all orders. We use the 1S mass scheme [27,28]. The corresponding expression for δm_t at NLL order can also be found in Ref. [17]. We use the 1S top quark mass and implement the residual mass term in the soft factor of the factorization formula because it avoids the pole mass renormalon problem [29] and leads to a $t\bar{t}$ resonance peak position that is stable under higher order perturbative corrections [30]. For the NLL order QCD corrections to the hard factors, which are discussed below, we neglect the corrections that arise from the residual mass term because the numerical effects are at the 1% level and substantially smaller than the uncertainties from low-energy QCD effects. This approximation was also used in Ref. [17].

Concerning the hard contributions in Eq. (3), the first term in the parenthesis gives the contribution for the $t\bar{t}$ pair in a S-wave spin singlet state and the other three terms give the contributions for the $t\bar{t}$ pair in the three S-wave spin triplet $(+1, 0, -1)$ states. As described already in Ref. [17] we use the helicity basis for the top and antitop spinors in the endpoint where $k_1 = k_2$ (see Fig. 1) to define the singlet and the triplet states. In this basis there are additional ν-suppressed (NLL) contributions to the triplet ± 1 contribution that arise from S-P wave interference terms and originate from the interference of vector and axial-vector contributions at the $t\bar{t}$ vertex. These additional order

ν contributions cancel in the sum of the triplet contributions and can also be avoided if a spin basis is used that does not depend on the momenta of the top quarks [31]. Since here we are not interested in the phenomenology of

top polarization these additional NLL order contributions are not included in Eq. (3). The functions $F^{Z, \gamma Z}$ are the tree-level (hard) matching conditions for the contributions of the respective $t\bar{t}$ spin states. They read

$$
\begin{aligned}
F^{\gamma, Z}_{(1, +1), \pm} = F^{\gamma, Z}_{(1, -1), \pm} &= \frac{2\alpha^2 \lambda_t^2}{6} \frac{(1 - x_H + 4x_t)^2}{(1 + x_H - 4x_t)^2} \left(Q_e^2 Q_t^2 + \frac{v_t^2 (v_e \mp a_e)^2}{(1 - x_Z)^2} + \frac{2Q_e Q_t (v_e \mp a_e) v_t}{(1 - x_Z)} \right) \\
&+ \frac{4\alpha^2 g_Z \lambda_t}{3} \frac{(x_t x_Z)^{1/2}(1 - x_H + 4x_t)}{(1 + x_H - 4x_t)(4x_t - x_Z)(1 - x_Z)} \left(\frac{v_t^2 (v_e \mp a_e)^2}{(1 - x_Z)} + Q_e Q_t (v_e \mp a_e) v_t \right) \\
&+ \frac{4\alpha^2 g_Z^2 v_t^2 (v_e \mp a_e)^2}{3} \frac{x_t x_Z}{(4x_t - x_Z)^2(1 - x_Z)^2},
\end{aligned} \tag{10}
$$

$$
\begin{aligned}
F^{\gamma, Z}_{(1, 0), \pm} &= \frac{16\alpha^2 \lambda_t^2}{3} \frac{x_t}{(1 + x_H - 4x_t)^2} \left(Q_e^2 Q_t^2 + \frac{v_t^2 (v_e \mp a_e)^2}{(1 - x_Z)^2} + \frac{2Q_e Q_t (v_e \mp a_e) v_t}{(1 - x_Z)} \right) \\
&+ \frac{4\alpha^2 g_Z \lambda_t}{3} \frac{(x_t x_Z)^{1/2}(1 - x_H + 4x_t)}{(1 + x_H - 4x_t)(4x_t - x_Z)(1 - x_Z)} \left(\frac{v_t^2 (v_e \mp a_e)^2}{(1 - x_Z)} + Q_e Q_t (v_e \mp a_e) v_t \right) \\
&+ \frac{\alpha^2 g_Z^2 v_t^2 (v_e \mp a_e)^2}{12} \frac{(1 - x_H + 4x_t)^2 x_Z}{(4x_t - x_Z)^2(1 - x_Z)^2},
\end{aligned} \tag{11}
$$

$$
F^Z_{0, \pm} = \frac{\alpha^2 g_Z^2 a_t^2 (v_e \mp a_e)^2}{12} \frac{(1 - x_H + 4x_t)^2 - 16x_t}{(1 - x_Z)^2 x_Z}, \tag{12}
$$

where

$$
v_f = \frac{T_3^f - 2Q_f s_w^2}{2s_w c_w}, \qquad a_f = \frac{T_3^f}{2s_w c_w},
$$
$$
\lambda_t = \frac{e}{2s_w} \frac{m_t}{M_W}, \qquad g_Z = \frac{e}{2s_w c_w}, \qquad \alpha = \frac{e^2}{4\pi}. \tag{13}
$$

Here, Q_f and T_3^f are the fermion charge and weak isospin, e is the electric charge and s_w (c_w) the sine (cosine) of the Weinberg angle.

The functions $c_i(\nu)$ are the hard QCD Wilson coefficients and depend on m_t, m_H and the c.m. energy $\sqrt{s}$. They also depend on the renormalization parameter ν which accounts for the renormalization group running of the effective currents that produce and annihilate the $t\bar{t}$ pair in the various S-wave spin states. To achieve reliable predictions the renormalization scaling parameter ν has to be chosen of order α_s, i.e. of order of the average top velocity in the $t\bar{t}$ c.m. system. For this choice the imaginary part of the zero-distance Green function does not contain any large logarithms from ratios of the hard scales and the small nonrelativistic scales, the top three momentum $\mathbf{p}_t \sim m_t \nu$ and the top kinetic energy $E_t \sim m_t \nu^2$ defined in the $t\bar{t}$ c.m. system. All large logarithms are summed into the hard QCD coefficients. At NLL order the renormalization group evolution of the hard QCD coefficients can be parameterized as

$$
c_{(1, i), \pm}(\nu) = c_{(1, i), \pm}(1) \exp(f(\nu, 2)), \qquad (i = 0, \pm 1)
$$
$$
c_0(\nu) = c_0(1) \exp(f(\nu, 0)). \tag{14}
$$

The function f was given in Ref. [17] using the results obtained in Refs. [19,32]. Whereas the renormalization group running of the coefficients can be determined within the effective theory, and is independent of the short distance process, the matching conditions at $\nu = 1$ are process-dependent. We use the convention that the LL matching conditions for the $c_i(\nu)$ are normalized to unity. At NLL order the matching conditions are obtained from matching the factorization formula expanded to order α_s to the corresponding full theory Higgs energy distribution at $\mathcal{O}(\alpha_s)$ in the endpoint region expanded to $\mathcal{O}(\nu)$ for stable top quarks and using $\nu = 1(\mu = m_t)$ for the renormalization scaling parameters. The full theory predictions are taken from the numerical codes obtained in Ref. [15]. More information on the numerical matching procedure can be found in Ref. [17]. The NLL matching conditions can be parameterized in the form

$$
c_{(1, i), \pm}(\nu = 1) = 1 + \frac{C_F \alpha_s(m_t)}{2} \delta c_{(1, i), \pm}(\sqrt{s}, m_t, m_H),
$$
$$
(i = 0, \pm 1)
$$
$$
c_{1, \pm}(\nu = 1) = 1 + \frac{C_F \alpha_s(m_t)}{2} \delta c_{1, \pm}(\sqrt{s}, m_t, m_H),
$$
$$
c_0(\nu = 1) = 1 + \frac{C_F \alpha_s(m_t)}{2} \delta c_0(\sqrt{s}, m_t, m_H), \tag{15}
$$

and numerical results for the NLL order contributions for various choices of $\sqrt{s}$, m_t and m_H are given in Table I.

TABLE I.   Numerical values for the matching conditions for the singlet and triplet hard QCD coefficients for typical values $\sqrt{s}$, m_t and m_H. The masses and energies are given in units of GeV. Note that $c_{(1,+1),\pm} = c_{(1,-1),\pm}$ due to parity.

$\sqrt{s}$	m_t	m_H	$\delta c_{1,+}$	$\delta c_{1,-}$	$\delta c_{(1,\pm 1),+}$	$\delta c_{(1,\pm 1),-}$	$\delta c_{(1,0),+}$	$\delta c_{(1,0),-}$	δc_0
500	170	115	−2.3011(2)	−2.2703(2)	−2.2954(2)	−2.2654(2)	−2.3134(2)	−2.2807(2)	−0.573(4)
490	170	115	−2.2910(4)	−2.2618(4)	−2.2867(4)	−2.2581(4)	−2.3001(4)	−2.2695(4)	−0.565(5)
480	170	115	−2.2804(7)	−2.2528(7)	−2.2775(7)	−2.2503(7)	−2.2866(7)	−2.2581(7)	−0.557(6)
470	170	115	−2.2689(5)	−2.2430(5)	−2.2672(5)	−2.2415(5)	−2.2724(5)	−2.2460(5)	−0.547(9)
460	170	115	−2.257(1)	−2.232(1)	−2.256(1)	−2.232(1)	−2.258(1)	−2.233(1)	−0.54(1)
500	170	120	−2.2992(4)	−2.2681(4)	−2.2940(4)	−2.2637(4)	−2.3105(4)	−2.2776(4)	−0.572(4)
490	170	120	−2.2890(6)	−2.2596(6)	−2.2852(6)	−2.2563(6)	−2.2971(6)	−2.2664(6)	−0.564(5)
480	170	120	−2.2779(4)	−2.2501(4)	−2.2754(4)	−2.2479(4)	−2.2830(4)	−2.2544(4)	−0.555(4)
470	170	120	−2.2660(9)	−2.2399(9)	−2.2648(9)	−2.2389(9)	−2.2684(9)	−2.2419(9)	−0.546(9)
500	170	140	−2.2931(6)	−2.2610(6)	−2.2901(6)	−2.2584(6)	−2.2994(6)	−2.2663(6)	−0.568(9)
490	170	140	−2.2815(6)	−2.2510(6)	−2.2800(6)	−2.2498(6)	−2.2845(6)	−2.2536(6)	−0.559(9)
500	175	115	−2.2871(3)	−2.2605(3)	−2.2831(3)	−2.2571(3)	−2.2956(3)	−2.2678(3)	−0.562(2)
490	175	115	−2.2767(4)	−2.2516(4)	−2.2740(4)	−2.2492(4)	−2.2824(4)	−2.2565(4)	−0.554(2)
480	175	115	−2.2657(6)	−2.2421(6)	−2.2641(6)	−2.2407(6)	−2.2689(6)	−2.2449(6)	−0.544(9)
470	175	115	−2.2536(9)	−2.2315(9)	−2.2531(9)	−2.2311(9)	−2.2546(9)	−2.2324(9)	−0.54(1)
500	175	120	−2.2848(5)	−2.2580(5)	−2.2813(5)	−2.2550(4)	−2.2923(4)	−2.2645(4)	−0.561(5)
490	175	120	−2.2741(5)	−2.2488(5)	−2.2719(5)	−2.2469(5)	−2.2789(5)	−2.2529(5)	−0.553(4)
480	175	120	−2.263(1)	−2.2389(8)	−2.2616(8)	−2.2380(8)	−2.265(1)	−2.2409(8)	−0.544(6)
500	175	140	−2.2766(5)	−2.2489(5)	−2.2752(5)	−2.2477(5)	−2.2793(5)	−2.2512(5)	−0.556(5)

The singlet matching conditions do not depend on the electron-positron polarization because there is only one nontrivial QCD form factor in the full theory that can contribute to the hard QCD matching conditions for the effective theory spin singlet $t\bar{t}$ current. In Feynman gauge it originates from the pseudoscalar Goldstone-$t\bar{t}$ vertex. For the triplet currents, on the other hand, several form factors contribute in the full theory $t\bar{t}$ vertices, therefore the matching conditions are polarization-dependent for the parameterization used in Eq. (3).

If the polarization of the $t\bar{t}$ final states is not accounted for, the factorization formula can be written in a simpler form using for the $t\bar{t}$ spin triplet contributions the definitions

$$c^2_{1,\pm}(\nu)F^{\gamma Z}_{1,\pm} \equiv \sum_{i=-1,0,+1} c^2_{(1,i),\pm}(\nu)F^{\gamma Z}_{(1,i),\pm},$$

$$F^{\gamma Z}_{1,\pm} \equiv \sum_{i=-1,0,+1} F^{\gamma Z}_{(1,i),\pm}, \qquad (16)$$

$$c^2_{1,\pm}(\nu) = \frac{\displaystyle\sum_{i=-1,0,+1} c^2_{(1,i),\pm}(\nu)F^{\gamma Z}_{(1,i),\pm}}{F^{\gamma Z}_{1,\pm}}.$$

In Ref. [17] the results for the triplet contributions were presented in this form.

III. THE LOW HIGGS ENERGY ENDPOINT REGION

In Fig. 2 the prediction for the unpolarized Higgs energy spectrum obtained from the factorization formula in Eq. (3) has been displayed at LL (dotted lines) and NLL (solid lines) order in the nonrelativistic expansion for the effective theory renormalization parameters $\nu = 0.1, 0.2, 0.4$. The parameters are $\sqrt{s} = 500$ GeV, $m_t^{1S} = 175$ GeV, $m_H = 120$ GeV, and
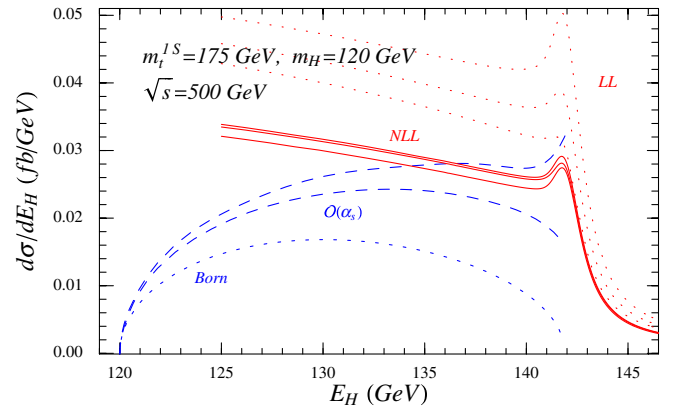

FIG. 2 (color online).   The unpolarized Higgs energy spectrum in the nonrelativistic expansion at LL (dotted lines) and NLL (solid lines) order for $\nu = 0.1, 0.2, 0.4$. The fixed-order expansion is also shown at Born level (lower dotted line) and at $\mathcal{O}(\alpha_s)$ for $\mu = \sqrt{s}$ (lower dashed line) at for $\mu = \sqrt{s}\nu$ (upper dashed line). The cross section at NLL order fails to reproduce the correct physical behavior of the fixed-order results from the loop expansion in the *low* Higgs energy regime. At the 1S peak the upper (lower) NLL order curve corresponds to the effective theory renormalization parameter $\nu = 0.2(0.1)$.

$$\Gamma_t = 1.43 \text{ GeV}, \qquad M_Z = 91.1876 \text{ GeV},$$

$$M_W = 80.423 \text{ GeV}, \qquad \alpha^{-1} = 137.036, \qquad (17)$$

$$c_w = M_W/M_Z.$$

We have also plotted the tree-level (lower dotted line) and the $\mathcal{O}(\alpha_s)$ Higgs energy spectrum for $\mu = \sqrt{s}$ (lower dashed line) and for $\mu = \sqrt{s}v$ (upper dashed line) where v is the $t\bar{t}$ relative velocity defined in Eq. (8). Since the hard scale as well as the relative momentum of the top quarks are scales that are relevant for nonrelativistic $t\bar{t}$ production, the difference between the two scale choices illustrates the ambiguity contained in the fixed-order calculation close to the large Higgs energy endpoint. A detailed discussion of the deficiencies of the fixed-order predictions in the endpoint region and quality of the nonrelativistic expansion and the theoretical normalization uncertainty of the NLL order prediction has been given in Ref. [17] and shall not be repeated here. The issue we want to point out in Fig. 2 is that the predictions obtained from the factorization formula in Eq. (3), which properly accounts for the summation of all NLL order contributions in the *large* Higgs energy region, is not compatible with the correct physical behavior at the *low* Higgs energy endpoint $E_H = m_H$. There the Higgs boson is produced at rest (in the lab frame) and the Higgs energy spectrum has to go to zero as do the

tree-level and $\mathcal{O}(\alpha_s)$ predictions. In particular, at the low Higgs energy endpoint region there is no singular enhancement from the matrix elements, and due to phase space suppression the coefficient functions G_i of e.g. the tree-level Higgs energy spectrum (see Appendix A) vanish like $G_i \sim \hat{\beta}$ with

$$\hat{\beta} = \left(\frac{m_H(\sqrt{s} - m_H)^2((\sqrt{s} - m_H)^2 - 4m_t^2)}{m_t^2 s^{3/2}} \right)^{1/2}$$

$$\times \sqrt{v_{\max}^2 - v^2} + \mathcal{O}(v_{\max}^2 - v^2)^{3/2}. \qquad (18)$$

This endpoint behavior cannot be obtained within the non-relativistic expansion in small v even if the endpoint is located at a velocity much smaller than 1, see Eq. (2). Terms that are formally from beyond NLL order in v thus need to be summed up to achieve a correct low Higgs energy endpoint behavior.

It is useful for the construction of a factorization formula which can account for the correct physical low Higgs energy behavior that the full theory tree-level Higgs energy spectrum, both for the $t\bar{t}$ pair in the spin singlet and for the (combined) triplet configuration, does not have order v (NLL) corrections to the leading endpoint behavior in the large Higgs energy endpoint, i.e.

$$\left(\frac{d\sigma}{dE_H}(E_H \approx E_H^0) \right)_{1,\text{Born}}^{\pm} = \left[\frac{2N_c[(1 + x_H - 4x_t)^2 - 4x_H]^{1/2}}{s^{3/2}\pi} F_{1,\pm}^{\gamma Z} \right] v + \mathcal{O}(v^3),$$

$$\left(\frac{d\sigma}{dE_H}(E_H \approx E_H^0) \right)_{0,\text{Born}}^{\pm} = \left[\frac{2N_c[(1 + x_H - 4x_t)^2 - 4x_H]^{1/2}}{s^{3/2}\pi} F_{0,\pm}^{Z} \right] v + \mathcal{O}(v^3). \qquad (19)$$

At NLL order it is thus consistent to use the full tree-level E_H spectrum in the large Higgs energy endpoint instead of the constant LL matching conditions $F^{Z,\gamma,Z}$ given in Eqs. (10)–(12),

$$F_{1,\pm}^{\gamma Z} \rightarrow \left(\frac{d\sigma}{dE_H} \right)_{\text{Born}}^{\pm} \frac{F_{1,\pm}^{\gamma Z}}{F_{0,\pm}^{\gamma Z} + F_{1,\pm}^{\gamma Z}} \left[\frac{2N_c[(1 + x_H - 4x_t)^2 - 4x_H]^{1/2}}{s^{3/2}\pi} v \right]^{-1},$$

$$F_{0,\pm}^{Z} \rightarrow \left(\frac{d\sigma}{dE_H} \right)_{\text{Born}}^{\pm} \frac{F_{0,\pm}^{Z}}{F_{0,\pm}^{Z} + F_{1,\pm}^{\gamma Z}} \left[\frac{2N_c[(1 + x_H - 4x_t)^2 - 4x_H]^{1/2}}{s^{3/2}\pi} v \right]^{-1}, \qquad (20)$$

where $(\frac{d\sigma}{dE_H})_{\text{Born}}^{\pm}$ is the full tree-level Higgs energy spectrum for the polarized e^+e^- initial state. Note that the replacement prescription in Eq. (20) can only be applied for Higgs energies smaller than E_H^0, for larger Higgs energies Eq. (3) is left unchanged. For the convenience of the reader we have given the analytic expressions for the tree-level Higgs energy spectrum in the appendix using up to minor modifications the conventions of Ref. [13]. They also correct a few typos that were contained in Ref. [13] and pointed out before in Ref. [17]. For the case of an unpolarized $t\bar{t}$ final state, using the prescription (20) in the factorization formula (3) leads to a modified factorization formula that resums correctly all NLL order terms. In addition it has

the correct physical behavior at the low Higgs energy endpoint $E_H = m_H$.

The modified NLL factorization formula based on Eqs. (3), (16), and (20) is not unique, alternative prescriptions to achieve the correct physical low Higgs energy endpoint behavior are conceivable. However, different prescriptions will only affect the low Higgs energy endpoint where the E_H spectrum vanishes, and they should therefore not have a large numerical impact. While the modified NLL factorization formula contains the exact tree-level contribution, its $\mathcal{O}(\alpha_s)$ contribution (in the expansion in powers of α_s) differs from the exact $\mathcal{O}(\alpha_s)$ result obtained in Ref. [15] since it includes only the QCD corrections of

the large Higgs energy endpoint. Thus an estimate of the intrinsic uncertainty in our prescription can be gained by comparing its $\mathcal{O}(\alpha_s)$ terms with the exact result from Refs. [11,15]. For stable and unpolarized top quarks the first two terms in the α_s expansion of our modified factorization formula read

$$\left(\frac{d\sigma}{dE_H}(E_H)\right)^{\pm}_{\mathrm{NLL}} = \left(\frac{d\sigma}{dE_H}(E_H)\right)^{\pm}_{\mathrm{Born}} + \left(\frac{d\sigma}{dE_H}(E_H)\right)^{\pm}_{\mathcal{O}(\alpha_s)}$$
$$+ \mathcal{O}(\alpha_s^2), \tag{21}$$

where

$$\left(\frac{d\sigma}{dE_H}(E_H)\right)^{\pm}_{\mathcal{O}(\alpha_s)} = C_F\alpha_s\left[\frac{F^Z_{0,\pm}\delta c_0 + F^{\gamma Z}_{1,\pm}\delta c_{1,\pm}}{F^Z_{0,\pm} + F^{\gamma Z}_{1,\pm}}\right.$$
$$\left. + \frac{\pi}{2}\left(1 - \frac{4m_t^2}{Q^2}\right)^{-1/2}\right]\left(\frac{d\sigma}{dE_H}(E_H)\right)^{\pm}_{\mathrm{Born}}.$$
$$\tag{22}$$

In Table II numerical results for the exact total $\mathcal{O}(\alpha_s)$ unpolarized cross section, $\sigma^{\mathcal{O}(\alpha_s)}_{\mathrm{exact}}$ [15], and for the $\mathcal{O}(\alpha_s)$ approximation from Eq. (21), $\sigma^{\mathcal{O}(\alpha_s)}_{\mathrm{NLL}}$, are shown for various c.m. energies and $m_t = 175$ GeV, $m_H = 120$ GeV, $\Gamma_t = 0$, $\mu = \sqrt{s}$. For c.m. energies below 500 GeV the deviation increases with the c.m. energy. It vanishes at the three-body threshold $\sqrt{s} \approx 2m_t + m_H$ and reaches the level of 1.5% for $\sqrt{s} = 500$ GeV.

In Fig. 3 the exact $\mathcal{O}(\alpha_s)$ unpolarized Higgs energy spectrum (black lines) and the $\mathcal{O}(\alpha_s)$ approximation in Eq. (21) (gray lines) are displayed in 0.1 GeV bins for $\sqrt{s} = 490, 500, 600,$ and 700 GeV, $m_t = 175$ GeV, $m_H = 120$ GeV, $\Gamma_t = 0$, and $\mu = \sqrt{s}$. Note that for the strong coupling we use $\alpha_s(500$ GeV$) = 0.09396$. The other parameters are chosen as in Eq. (17). For $\sqrt{s} = 500$ GeV the relative deviation in the Higgs energy spectrum is at most 2.8%. The difference is smaller for lower c.m. energies since the maximal possible top relative velocity v^{max} is increasing with the c.m. energy, see Eq. (2). The results indicate that the intrinsic uncertainty of our approach is

TABLE II.　The total cross section using the exact $\mathcal{O}(\alpha_s)$ result $\sigma^{\mathcal{O}(\alpha_s)}_{\mathrm{exact}}$ from Ref. [15] and the approximation based on Eq. (21), $\sigma^{\mathcal{O}(\alpha_s)}_{\mathrm{NLL}}$. The third column shows the relative deviation in percent. The difference between the two calculations is maximal for c.m. energies around 550 GeV.

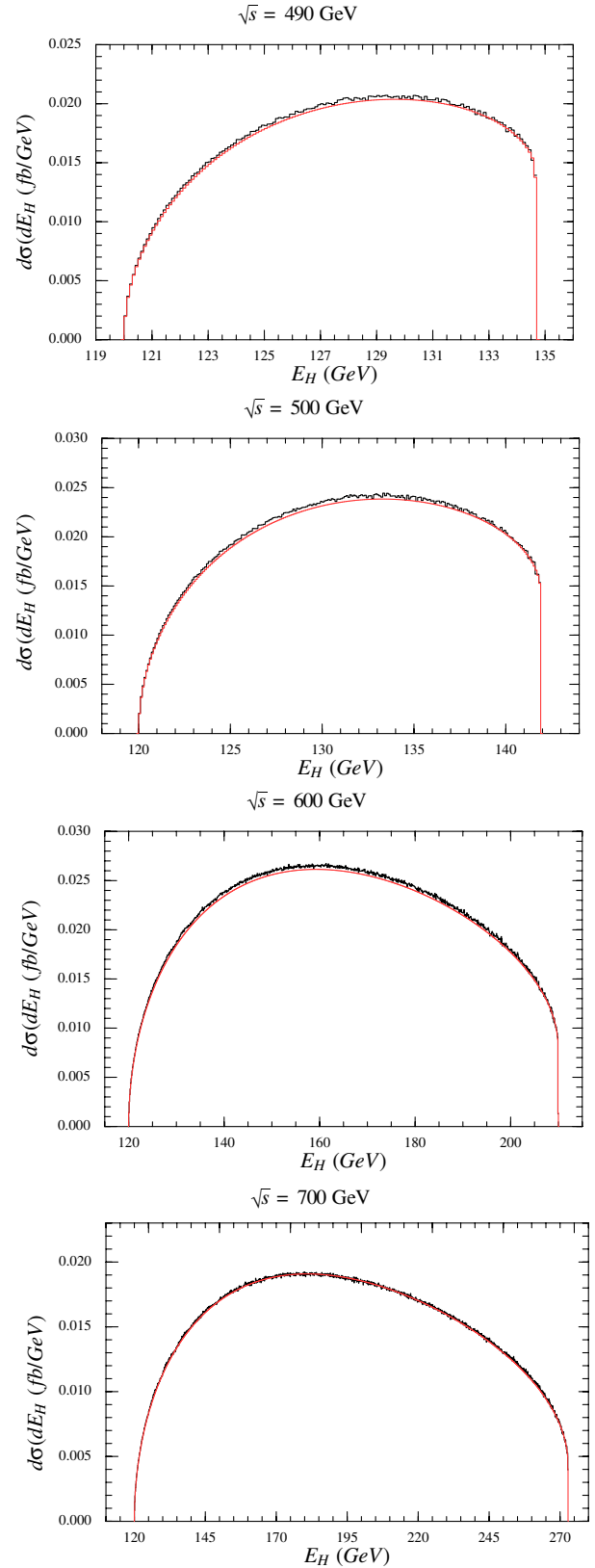| $\sqrt{s}$	$\sigma^{\alpha_s}_{\mathrm{exact}}$	$\sigma^{\alpha_s}_{\mathrm{NLL}}$	rel. dev. (%)
475	0.0311	0.0309	0.6
480	0.0908	0.0900	0.9
490	0.254	0.251	1.2
500	0.446	0.439	1.5
550	1.366	1.343	1.7
600	1.953	1.924	1.5
700	2.356	2.348	0.4

FIG. 3 (color online).　The exact $\mathcal{O}(\alpha_s)$ unpolarized Higgs energy spectrum from Ref. [15] (black lines) and the $\mathcal{O}(\alpha_s)$ approximation in Eq. (21) (gray lines) for different c.m. energies $\sqrt{s}$ for $m_t = 175$ GeV, $m_H = 120$ GeV, and $\mu = \sqrt{s}$.

substantially smaller than the theoretical uncertainty of 5% from uncalculated higher order QCD effects [17,25].

In Figs. 3(c) and 3(d) and in Table II we have analyzed the difference between the exact $\mathcal{O}(\alpha_s)$ results and the $\mathcal{O}(\alpha_s)$ approximation based on Eq. (21) for larger c.m. energies as well. It is a surprising fact that the fairly simple expression in Eq. (22), which contains only tree-level information and the NLL QCD information from the large Higgs energy endpoint, can also account very well for the exact $\mathcal{O}(\alpha_s)$ results at higher energies, where real gluon radiation is non-negligible. For c.m. energies between 500 and 700 GeV the approximation based on Eq. (21) deviates from the exact results by at most 1.8% for the unpolarized total cross section, where the maximal deviation is reached for $\sqrt{s} \approx 550$ GeV. Since the numerical evaluation of Eq. (22) is substantially faster than for the exact $\mathcal{O}(\alpha_s)$ result [15], it can be useful as an efficient approximation formula for higher c.m. energies.

IV. NUMERICAL ANALYSIS

In Fig. 4 the unpolarized Higgs energy spectrum at NLL order (solid lines) using the modified factorization formula based on Eqs. (3), (16), and (20) is displayed for the renormalization parameters $\nu = 0.1, 0.2, 0.4$ for the c.m. energies $\sqrt{s} = 485, 490, 495, 500$ GeV and $m_t = m_t^{1S} = 175$ GeV, $m_H = 120$ GeV. The other parameters are chosen as in Eq. (17). For comparison we also show the tree-level prediction (dotted lines) and the $\mathcal{O}(\alpha_s)$ results [15] (dashed lines) with $\mu = \sqrt{s}$ for a stable top quark. The nonrelativistic NLL order results show a substantial enhancement compared to the tree-level and one-loop QCD

predictions. The Higgs energy spectrum in the effective theory extends beyond the endpoint E_H^0 that is obtained for the stable top quark case. This is because the top quarks can be produced off-shell with invariant masses smaller than m_t if the top quark decay is accounted for. With the present technology the finite top quark lifetime can only be implemented systematically in an expansion in the top quark off-shellness, which is naturally provided by the nonrelativistic expansion we use here.

It is conspicuous that the spectrum above the endpoint E_H^0 in the NLL prediction falls off quite slowly. Since the average c.m. top quark velocity increases with the Higgs energy for $E_H > E_H^0$ we define the total cross section by applying a cut on the Higgs energy above E_H^0 such that the average c.m. top velocity remains below $v_{\text{cut}} = 0.2$. We fix the relation between the maximal Higgs energy and v_{cut} by the relation $E_H^{\text{cut}} = (s + m_H^2 - Q_{\text{cut}}^2)/(2\sqrt{s})$, which is exact in the stable top case. Here, $Q_{\text{cut}}^2 \equiv (4m_t^2)/(1 + v_{\text{cut}}^2)$ is the minimal $t\bar{t}$ invariant mass. Note that Q_{cut} is smaller than $2m_t$ because for $E_H > E_H^0$ we are in the bound state regime. As mentioned before, we plan a systematic treatment of finite lifetime and off-shell effects at the NLL order level in a subsequent publication.

In Table III the impact of the NLL order summations on the total cross section for unpolarized $t\bar{t}$ pairs and polarized electron-positron beams is analyzed numerically for various c.m. energies, top quark masses and Higgs masses. The other parameters are chosen as in Eq. (17) except for the case $m_t = 170$ GeV where we use $\Gamma_t = 1.31$ GeV.

In Table III, σ_{Born} refers to the tree-level cross section for stable top quarks (see the appendix for explicit expressions) and σ_{NLL} to the NLL total cross section as defined
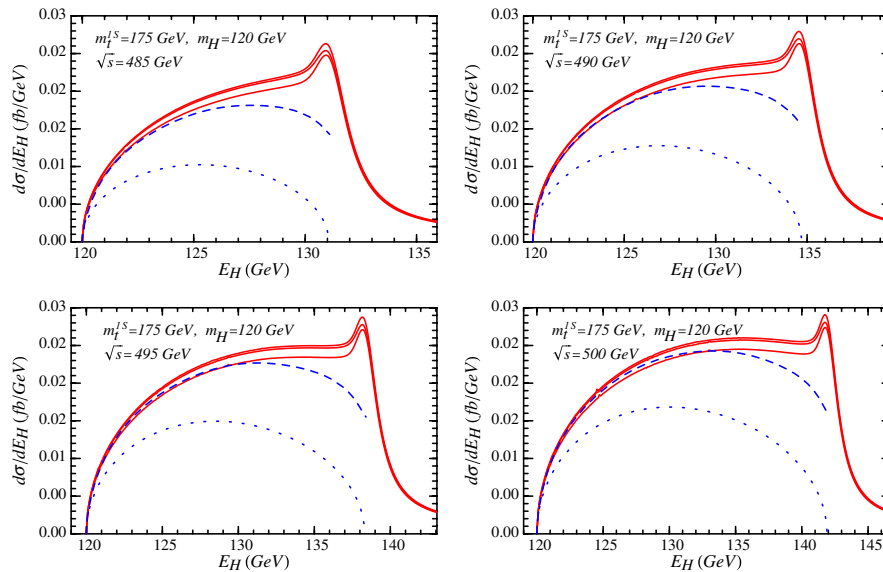

FIG. 4 (color online).   The unpolarized Higgs energy spectrum for different c.m. energies at NLL order (solid lines) using the modified factorization formula based on Eqs. (3), (16), and (20) for the renormalization parameters $\nu = 0.1, 0.2, 0.4$, at $\mathcal{O}(\alpha_s)$ (dashed lines) from Ref. [11] with $\mu = \sqrt{s}$, and at Born level (dotted line). At the 1S peak the upper (lower) NLL order curve corresponds to the effective theory renormalization parameter $\nu = 0.2(0.1)$.

TABLE III.   The total cross section in units of fb at Born level for stable top quarks and at NLL order for unstable top quarks using $\nu = 0.2$ for fully polarized electron-positron beams. The index refers to the polarization of the electron beam. The masses and $\sqrt{s}$ are given in units of GeV. For $m_t = (170, 175)$ GeV we use $\Gamma_t = (1.31, 1.43)$ GeV.

$\sqrt{s}$	m_t	m_H	σ^+_{Born} (fb)	σ^+_{NLL} (fb)	$\sigma^+_{\text{NLL}}/\sigma^+_{\text{Born}}$	σ^-_{Born} (fb)	σ^-_{NLL} (fb)	$\sigma^-_{\text{NLL}}/\sigma^-_{\text{Born}}$
500	170	115	0.644	0.989(49)	1.54	1.660	2.568(128)	1.55
490	170	115	0.444	0.754(37)	1.70	1.149	1.965(98)	1.71
480	170	115	0.260	0.516(25)	1.98	0.674	1.347(67)	2.00
470	170	115	0.108	0.285(14)	2.64	0.281	0.747(37)	2.66
460	170	115	0.014	0.086(4)	6.17	0.036	0.226(11)	6.21
500	170	120	0.486	0.783(39)	1.61	1.258	2.040(101)	1.62
490	170	120	0.312	0.568(28)	1.82	0.809	1.483(74)	1.83
480	170	120	0.159	0.355(17)	2.23	0.413	0.929(46)	2.25
470	170	120	0.046	0.159(7)	3.48	0.120	0.418(20)	3.50
500	170	140	0.102	0.229(11)	2.24	0.268	0.604(30)	2.26
490	170	140	0.029	0.101(5)	3.48	0.076	0.268(13)	3.51
500	175	115	0.459	0.787(39)	1.72	1.181	2.039(101)	1.73
490	175	115	0.268	0.538(26)	2.01	0.692	1.399(69)	2.02
480	175	115	0.111	0.298(14)	2.68	0.288	0.777(38)	2.70
470	175	115	0.014	0.091(4)	6.32	0.037	0.236(11)	6.35
500	175	120	0.322	0.593(29)	1.84	0.832	1.541(77)	1.85
490	175	120	0.164	0.371(18)	2.26	0.425	0.967(48)	2.28
480	175	120	0.047	0.167(8)	3.54	0.123	0.437(21)	3.56
500	175	140	0.030	0.107(5)	3.55	0.079	0.281(14)	3.57

above and based on the modified factorization formula discussed in Sec. III. The NLL order predictions were obtained for the effective theory renormalization parameter $\nu = 0.2$. The uncertainties given for σ_{NLL} reflect the 5% theoretical error from higher order QCD and relativistic corrections as discussed in Ref. [17]. The results in Table III demonstrate the importance of the summation of the singular terms proportional to $(\alpha_s/\nu)^n$ and $(\alpha_s \ln\nu)^n$ that arise in the endpoint region, and of the off-shell effects that arise from the finite top quark lifetime. Compared to the tree-level predictions the enhancement is more pronounced for smaller c.m. energies and larger top or Higgs masses.

It is a realistic option for the ILC project to polarize the $e^+ e^-$ beams up to $(P_+, P_-) = (0.6, -0.8)$ [3]. Since this can further enhance the cross section we have also assessed its merits for the process at hand. In Figs. 5 the total cross section for unpolarized top quarks at the tree-level (dashed lines) and at NLL order (solid lines) is shown as a function of $\sqrt{s}$ and m_H for unpolarized electron-positron beams $(P_+, P_-) = (0, 0)$ and for $(P_+, P_-) = (0.6, -0.8)$. The other parameters are chosen as in Eq. (17), see also the figure caption for more details. For the NLL cross section the predictions for the three choices $\nu = 0.1, 0.2, 0.4$ for the renormalization scaling parameter are shown.

The results demonstrate that using electron-positron polarization the cross section can be enhanced by roughly a factor of 2 over the unpolarized cross section. Compared to the tree-level predictions for unpolarized electron-positron beams, which were the basis of previous experi-
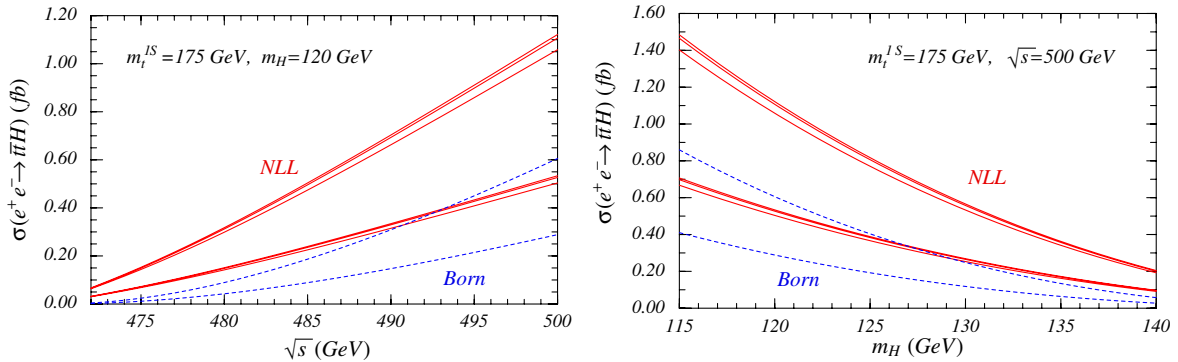

FIG. 5 (color online).   The total cross section for unpolarized top quarks at tree-level (dashed lines) and at NLL order (solid lines) as a function of $\sqrt{s}$ (left panel) and as a function of m_H (right panel) for unpolarized electron-positron beams $(P_+, P_-) = (0, 0)$ (respective lower curves) and for $(P_+, P_-) = (0.6, -0.8)$ (respective upper curves).

mental analyses [21], QCD effects and beam polarization $(P_+, P_-) = (0.6, -0.8)$ can enhance the cross section by about a factor of 4 or even more for $\sqrt{s} = 500$ GeV, depending on the Higgs mass. Because of the limited statistics for $t\bar{t}H$ production during the first phase of the ILC project, these results are important for realistic experimental simulations of Yukawa coupling measurements.

V. CONCLUSION

We have analyzed the impact of summing the QCD singularities proportional to $(\alpha_s/v)^n$ and $(\alpha_s \ln v)^n$ that arise in the large Higgs energy endpoint region for the process $e^+ e^- \to t\bar{t}H$ for c.m. energies up to 500 GeV, i.e. energies which can be achieved during the first phase of the ILC project. The singularities cause the breakdown of usual multiloop perturbation theory in powers of α_s and originate from nonrelativistic dynamical QCD effects that arise because the relative velocity of the $t\bar{t}$ pair is small. A consistent theoretical treatment requires the use of nonrelativistic effective theory methods and includes a systematic treatment of off-shell effects caused by the finite top quark lifetime. In Ref. [17] we derived a factorization formula for the large Higgs energy endpoint region for large c.m. energies above 500 GeV. In the present work we have extended the approach to c.m. energies below 500 GeV, where the top quark pair is nonrelativistic in the entire phase space, and we have also accounted for the effects of electron-positron beam polarization. We have determined the predictions for the Higgs energy spectrum and the total cross section at NLL order for the QCD effects and at LL order for the top quark finite lifetime and for off-shell effects. The QCD effects enhance the total cross section by roughly a factor of 2 relative to the Born prediction for $\sqrt{s} = 500$ GeV. Using polarized electron-positron beams the cross section can be further enhanced over the unpolarized case by another factor of approximately two. Our results are important for realistic simulation studies for Yukawa coupling measurements in the first phase of the ILC project.

APPENDIX: TREE-LEVEL HIGGS ENERGY SPECTRUM

Correcting the typos of Ref. [13] the tree-level Higgs energy spectrum in the process $e^+ e^- \to t\bar{t}H$ for polarized electron-positron beams reads ($x_E \equiv 2E_H/\sqrt{s}$, $\sigma_{\text{pt}} \equiv 4\pi\alpha^2/(3s)$)

$$\left(\frac{d\sigma(E_H)}{dx_E}\right)^{\pm}_{\text{Born}} = \sigma_{\text{pt}} \frac{N_c}{8\pi^2} \left\{ \left[Q_e^2 Q_t^2 + \frac{2Q_e Q_t (v_e \mp a_e) v_t}{1 - x_Z} \right. \right.$$
$$\left. + \frac{(v_e \mp a_e)^2 (v_t^2 + a_t^2)}{(1 - x_Z)^2} \right] G_1$$
$$+ \frac{(v_e \mp a_e)^2}{(1 - x_Z)^2} \left[a_t^2 \sum_{i=2}^{6} G_i + v_t^2 (G_4 + G_6) \right]$$
$$\left. + \frac{Q_e Q_t (v_e \mp a_e) v_t}{1 - x_Z} G_6 \right\}, \tag{A1}$$

where the coefficient functions are given by

$$G_1 = \frac{2\lambda_t^2}{(\hat{\beta}^2 - x_E^2) x_E} \left\{ -4\hat{\beta}(4x_t - x_H)(2x_t + 1) x_E \right.$$
$$+ (\hat{\beta}^2 - x_E^2)[16x_t^2 + 2x_H^2 - 2x_H x_E + x_E^2$$
$$\left. - 4x_t(3x_H - 2 - 2x_E)] \ln\left(\frac{x_E + \hat{\beta}}{x_E - \hat{\beta}}\right) \right\}, \tag{A2}$$

$$G_2 = \frac{-2\lambda_t^2}{(\hat{\beta}^2 - x_E^2) x_E} \left\{ \hat{\beta} x_E [-96x_t^2 + 24x_t x_H - (-x_H + 1 \right.$$
$$+ x_E)(x_E^2 - \hat{\beta}^2)] + 2(\hat{\beta}^2 - x_E^2)[24x_t^2 + 2(x_H^2$$
$$\left. - x_H x_E) + x_t(-14x_H + 12x_E + x_E^2)] \ln\left(\frac{x_E + \hat{\beta}}{x_E - \hat{\beta}}\right) \right\}. \tag{A3}$$

These first two coefficients describe the s-channel exchange of the photon and the Z boson where the Higgs boson is radiated off one of the top quarks [13]. A missing factor s is introduced in the first line of the formula for G_2.

The coefficient functions G_3 to G_6 describe the emission of the Higgs boson from the Z-boson,

$$G_3 = \frac{-2\hat{\beta} g_Z^2 x_t}{x_Z(x_H - x_Z + 1 - x_E)^2} \left\{ 4x_H^2 + 12x_Z^2 + 2x_Z x_E^2 \right.$$
$$\left. + (-1 + x_E)x_E^2 - x_H[8x_Z + (-4 + 4x_E + x_E^2)] \right\}, \tag{A4}$$

$$G_4 = \frac{\hat{\beta} g_Z^2 x_Z}{6(x_H - x_Z + 1 - x_E)^2} \left\{ 48x_t + 12x_H \right.$$
$$\left. - (-24 + \hat{\beta}^2 + 24x_E - 3x_E^2) \right\}, \tag{A5}$$

$$G_5 = \frac{4\lambda_t g_Z x_t^{1/2}}{x_Z^{1/2}(-x_H + x_Z - 1 + x_E)} \left\{ \hat{\beta}[6x_Z \right.$$
$$+ x_E(-x_H - 1 + x_E)] + 2[x_H(x_H - 3x_Z$$
$$\left. + 1 - x_E) + x_t(-4x_H + 12x_Z + x_E^2)] \ln\left(\frac{x_E + \hat{\beta}}{x_E - \hat{\beta}}\right) \right\}, \tag{A6}$$

$$G_6 = \frac{-8\lambda_t g_Z (x_t x_Z)^{1/2}}{-x_H + x_Z - 1 + x_E} \left\{ \hat{\beta} + (4x_t - x_H + 2 - x_E) \right.$$
$$\left. \times \ln\left(\frac{x_E + \hat{\beta}}{x_E - \hat{\beta}}\right) \right\}. \tag{A7}$$

These terms give contributions to the Higgs energy spectrum of less than a few percent in the energy range between 500 GeV and 1 TeV. The overall signs of G_5 and G_6 are changed relative to [13]. The couplings and constants are defined in Eqs. (4) and (13) and the term $\hat{\beta}$ is given by

$$\hat{\beta} = \left(\frac{4(E_H^2 - m_H^2)(E_H^0 - E_H)}{\sqrt{s}((E_H^0 - E_H)\sqrt{s} + 2m_t^2)} \right)^{1/2}, \tag{A8}$$

with the large Higgs energy endpoint being defined as

$$E_H^0 \equiv \frac{s + m_H^2 - 4m_t^2}{2\sqrt{s}}. \tag{A9}$$

[1] R. Barate *et al.* (ALEPH Collaboration), Phys. Lett. B **565**, 61 (2003).

[2] M. W. Grunewald, hep-ex/0511018.

[3] J. A. Aguilar-Saavedra *et al.* (ECFA/DESY LC Physics Working Group Collaboration), hep-ph/0106315.

[4] T. Abe *et al.* (American Linear Collider Working Group Collaboration), hep-ex/0106057; hep-ex/0106056.

[5] K. Abe *et al.* (ACFA Linear Collider Working Group Collaboration), hep-ph/0109166.

[6] T. E. W. Group, hep-ex/0603039.

[7] A. Juste and G. Merino, hep-ph/9910301.

[8] A. Gay, hep-ph/0604034.

[9] A. Djouadi, J. Kalinowski, and M. Spira, Comput. Phys. Commun. **108**, 56 (1998).

[10] K. J. F. Gaemers and G. J. Gounaris, Phys. Lett. B **77**, 379 (1978); A. Djouadi, J. Kalinowski, and P. M. Zerwas, Mod. Phys. Lett. A **7**, 1765 (1992); Z. Phys. C **54**, 255 (1992).

[11] S. Dittmaier, M. Kramer, Y. Liao, M. Spira, and P. M. Zerwas, Phys. Lett. B **441**, 383 (1998).

[12] S. Dawson and L. Reina, Phys. Rev. D **57**, 5851 (1998).

[13] S. Dawson and L. Reina, Phys. Rev. D **59**, 054012 (1999).

[14] G. Belanger *et al.*, Phys. Lett. B **571**, 163 (2003).

[15] A. Denner, S. Dittmaier, M. Roth, and M. M. Weber, Nucl. Phys. **B680**, 85 (2004).

[16] Y. You, W. G. Ma, H. Chen, R. Y. Zhang, S. Yan-Bin, and H. S. Hou, Phys. Lett. B **571**, 85 (2003).

[17] C. Farrell and A. H. Hoang, Phys. Rev. D **72**, 014007 (2005).

[18] M. Luke, A. Manohar, and I. Rothstein, Phys. Rev. D **61**, 074025 (2000).

[19] A. H. Hoang and I. W. Stewart, Phys. Rev. D **67**, 114020 (2003).

[20] A. H. Hoang, A. V. Manohar, I. W. Stewart, and T. Teubner, Phys. Rev. Lett. **86**, 1951 (2001); Phys. Rev. D **65**, 014014 (2002).

[21] A. Juste, Talk Presented at the Chicago Linear Collider Workshop, Chicago, USA, 2002, http://www.pas.rochester.edu/ orr/justelc.pdf.

[22] A. Juste *et al.*, hep-ph/0601112; A. Juste, hep-ph/0512246.

[23] M. Jeżabek, J. H. Kühn, and T. Teubner, Z. Phys. C **56**, 653 (1992).

[24] M. J. Strassler and M. E. Peskin, Phys. Rev. D **43**, 1500 (1991).

[25] A. H. Hoang, Acta Phys. Pol. B **34**, 4491 (2003).

[26] A. H. Hoang and C. J. Reisser, Phys. Rev. D **71**, 074022 (2005).

[27] A. H. Hoang, Z. Ligeti, and A. V. Manohar, Phys. Rev. Lett. **82**, 277 (1999); Phys. Rev. D **59**, 074017 (1999).

[28] A. H. Hoang and T. Teubner, Phys. Rev. D **60**, 114027 (1999).

[29] A. H. Hoang, M. C. Smith, T. Stelzer, and S. Willenbrock, Phys. Rev. D **59**, 114014 (1999); M. Beneke, Phys. Lett. B **434**, 115 (1998); A. Pineda, Ph.D. thesis, Univ. Barcelona, 1998.

[30] A. H. Hoang *et al.*, Eur. Phys. J. direct C **2**, 1 (2000).

[31] S. J. Parke and Y. Shadmi, Phys. Lett. B **387**, 199 (1996).

[32] A. Pineda, Phys. Rev. D **66**, 054022 (2002).